Surface plasmon hybridization and exciton coupling

Daniel E. Gómez,[1,2,*] Ann Roberts,[1] Timothy J. Davis,[2] and Kristy C. Vernon[3]
[1]*School of Physics, The University of Melbourne, Parkville, VIC 3010, Australia*
[2]*CSIRO, Materials Science and Engineering, Private Bag 33, Clayton, Victoria 3168, Australia*
[3]*School of Chemistry, Physics and Mechanical Engineering Queensland University of Technology, GPO Box 2434, Brisbane, QLD 4001, Australia*
(Received 20 December 2011; revised manuscript received 23 April 2012; published 9 July 2012)

We derive a semianalytical model to describe the interaction of a single photon emitter and a collection of arbitrarily shaped metal nanoparticles. The theory treats the metal nanoparticles classically within the electrostatic eigenmode method, wherein the surface plasmon resonances of collections of nanoparticles are represented by the hybridization of the plasmon modes of the noninteracting particles. The single photon emitter is represented by a quantum mechanical two-level system that exhibits line broadening due to a finite spontaneous decay rate. Plasmon-emitter coupling is described by solving the resulting Bloch equations. We illustrate the theory by studying model systems consisting of a single emitter coupled to one, two, and three nanoparticles, and we also compare the predictions of our model to published experimental data.

DOI: 10.1103/PhysRevB.86.035411 PACS number(s): 73.20.Mf

I. INTRODUCTION

The use of surface plasmons (collective electron oscillations that occur at metal/dielectric interfaces) to develop optoelectronic technologies has attracted much attention due to the subwavelength confinement of electromagnetic energy.[1,2] Current fabrication techniques such as lithographic methods and wet-chemistry synthetic approaches, allow for the development of integrated structures with novel optical properties that so far have found applications in surface enhanced Raman scattering spectroscopy,[3,4] enhanced optical transmission[5] and optical metamaterials with negative refraction.[6,7] A key problem common to many of these applications of plasmonics arises from the strong losses exhibited by metals. These losses mainly arise from internal mechanisms leading to dissipation (such as electron-phonon coupling) and radiative losses exhibited by metallic nanostructures.

Two methodologies can be proposed to overcome these limitations. One of these consists of designing subwavelength metallic structures wherein the surface plasmon resonances (SPRs) are strongly nonradiative in nature, a feat achieved by creating structures with *dark* plasmon modes.[8] A complication associated with this proposal is that dark modes cannot be directly excited in the far field and instead they require a light source in the near field such as a dipole emitter or complex illumination strategies. A second alternative (that has raised much debate[9,10]) is to incorporate a gain medium in the nanostructures to overcome absorptive losses in the metal.[11–13] Common to these two solutions is therefore the interaction of plasmonic structures with dipole emitters that raises the question of how to optimize the interaction of these light sources with surface plasmon resonances (both bright and dark).

In this paper, we present a semianalytical formalism that accounts for the interaction of a single polarizable dipole (such as an organic dye molecule, impurity center in diamond or a quantum dot) and a collection of arbitrarily shaped metallic nanoparticles (MNPs). This type of interaction has been studied extensively in the literature (for an early comprehensive study see Ref. 14) where most of the cases considered involve coupling between highly symmetric structures such as a planar film to a point dipole,[14] a dielectric sphere containing the polarizable dipole coupled to a metallic sphere,[15–20] or to an ellipsoid.[21] Recently, a boundary element method has been presented[22] wherein more general metallic structures can be considered.

The approach presented here allows for a simple and more intuitive picture to describe the interaction of dipole emitters and plasmonic structures. It is based on the electrostatic eigenmode method,[23] where the collective plasmon resonances of coupled nanoparticles of arbitrary shape are described as linear and symmetric combinations of those of the noninteracting particles, similar to the case of molecular orbitals.

II. THEORY

We model the polarizable dipole as a dielectric sphere with two electronic states (ground and excited), a system that we will refer to as a nanocrystal quantum dot (NQD). The optical response of a NQD in the presence of a nearby set of metal nanoparticles (MNPs) can be found by solving the optical Bloch equations, which involve a term proportional to the product of the electric dipole moment of the NQD and the total electric field $\vec{\mathbf{E}}'$ driving its electronic transitions (dipole approximation). To find this electric field, we now proceed to solve the electrostatic problem associated with the MNP-NQD interaction. We only consider the electrostatic case where all the relevant size scales (NQD diameter, size of MNP and relative center-to-center distance $|\vec{R}|$) are much smaller than λ, the wavelength of the applied electric field $\vec{E}_o = E_o \hat{n}_e \cos(\omega t)$. Furthermore, we assume the MNPs and NQD to be embedded in an uniform dielectric medium of permittivity $\epsilon_b = 2.25$, which simulates that of the experimentally relevant case of Poly(methyl methacrylate) a widely-used material in nano fabrication (in the visible).

Within the electrostatic eigenmode method (EEM),[23] the localized surface plasmon resonances (LSPRs) of subwavelength sized MNPs are described in terms of both a surface charge density $\sigma(\vec{\mathbf{r}})$ and its (source-free) normal modes $\sigma_p^m(\vec{\mathbf{r}})$:

$$\sigma(\vec{\mathbf{r}}) = \sum_{p,m} \tilde{a}_p^m \sigma_p^m(\vec{\mathbf{r}}), \tag{1}$$

where the coefficients in this expansion $\tilde{a}_p^m$ are the "excitation amplitude" of the mth normal mode of particle p in the set. In effect, this equation describes the "hybridization"[23,24] of the surface plasmon modes σ_p^m that occurs due to the excitation by an external electric field and the electrostatic interaction among the particles. For a given MNP geometry, the EEM gives a prescription whereby the set $\sigma_p^m(\vec{\mathbf{r}})$, along with surface dipole distributions $\tau_p^m(\vec{\mathbf{r}})$, are found as a solution to an eigenvalue equation.[25–27] In general, the eigenvalue γ_p^m is a shape-dependent quantity which takes on a value of $\gamma_p^{x,y,z} = 3$ for spheres (for each of the three degenerate dipole modes of this geometrical shape) and decreases as the aspect ratio of the MNP increases.

The magnitude of the excitation amplitudes depends on the total electric field applied to the MNP, which in the case of one MNP in close proximity to a single NQD, has the following contributions:

$$\tilde{a}_p^m = f_p^m(\omega) \oint \tau_p^m(\vec{\mathbf{r}}_i)\hat{n}_i \cdot [\vec{\mathbf{E}}_o + \vec{\mathbf{E}}_x(\vec{\mathbf{r}}_i)]\, dS_i = a_p^m + C_{px}^{md}\tilde{a}_x^d, \tag{2}$$

a statement of the fact that the surface plasmons on the MNPs can be excited by the external driving field $\vec{\mathbf{E}}_o$ with an excitation amplitude a_p^m and the field produced by the NQD $\vec{\mathbf{E}}_x$ (in the notation that we adopt, the subscript x denotes the contributions from the NQD) with an amplitude proportional to C_{px}^{md}, the "coupling constant" between the resonant mode m of the particle p and the dipole d of the dielectric sphere (NQD) (an expression for this coupling constant is given in Appendix IV). $f_p^m(\omega)$ is a frequency-dependent factor related to the polarizability of the mth resonance mode of the particle. The integrals are evaluated on the surface S of the nanoparticles and $\hat{n}_i$ is the normal at a point $\vec{\mathbf{r}}_i$.

a_x^d is the excitation amplitude of an isolated NQD (modeled as a dielectric sphere), which is given by[28]

$$a_x^d = \frac{\epsilon_b}{\sqrt{V_s}}\alpha(\omega, E_o)\hat{x}_k \cdot \vec{\mathbf{E}}_o, \tag{3}$$

where $k = x,y,z$. $\hat{x}_k$ is a unit vector in the direction of k, V_s is the volume of the sphere, and $\alpha(\omega)$ its polarizability. For a two-state system in a uniform electric field $\vec{\mathbf{E}}_o$, this polarizability is given by[29]

$$\alpha(\omega, E_o) = \frac{\mu^2}{\epsilon_b \hbar}\frac{(\tilde{\omega}_o - \omega)}{(\omega - \tilde{\omega}_o)(\omega - \tilde{\omega}_o^*) + \left(\Omega_o^2/2\right)}, \tag{4}$$

with μ the interband dipole moment of the electronic transition, $\tilde{\omega}_o = \omega_o - i\Gamma_o/2$ is the complex resonance frequency of the two-level system, $\Omega_o = 3\epsilon_b \mu E_o/[2\hbar(\epsilon_S + 2\epsilon_b)]$ is the Rabi frequency of the driving field, and ϵ_S the static dielectric constant of the bulk semiconductor material. The factor $3\epsilon_b/(\epsilon_S + 2\epsilon_b)$ takes into account local field corrections that arise from dielectric confinement within the sphere. Strictly speaking, near an exciton transition ϵ_S becomes frequency dependent and therefore this local field factor also becomes a function of frequency.[30] In order to keep the problem algebraically tractable, we have approximated this local field correction factor by its low frequency limit.

$\tilde{a}_x^d$, the excitation amplitude of the interacting NQD, can be expanded in an analogous manner to Eq. (2):

$$\begin{aligned}\tilde{a}_x^d &= \frac{\epsilon_b}{\sqrt{V_s}}[\alpha(\omega, E_o)\hat{x}_k \cdot \vec{\mathbf{E}}_o + \alpha(\omega, E)\hat{x}_k \cdot \vec{\mathbf{E}}] \\ &= a_x^d + \frac{\epsilon_b}{\sqrt{V_s}}\alpha(\omega, E)\hat{x}_k \cdot \vec{\mathbf{E}} \\ &= a_x^d + C_{xp}^{dm}\tilde{a}_p^m,\end{aligned} \tag{5}$$

with an implicitly defined coupling coefficient C_{xp}^{dm}.

The electric field $\vec{\mathbf{E}}$ that appears in Eq. (5) is the one produced by the LSPR and is given by Coulomb's law:

$$\begin{aligned}\vec{\mathbf{E}}(\vec{\mathbf{r}}) &= \tilde{a}_p^m(\omega)\left[\frac{1}{4\pi\epsilon_b}\oint \sigma_p^m(\vec{\mathbf{r}}')\frac{(\vec{\mathbf{r}} - \vec{\mathbf{r}}')}{|\vec{\mathbf{r}} - \vec{r}'|^3}dS\right], \\ &= \tilde{a}_p^m(\omega)\vec{\mathbf{E}}_p^m(\vec{\mathbf{r}}),\end{aligned} \tag{6}$$

where the electric field per LSP mode $\vec{\mathbf{E}}_p^m(\vec{\mathbf{r}})$ has been defined as the quantity in square brackets.

Equation (5) together with Eq. (2) results in a system of two equations for the excitation amplitudes of the interacting MNP-NQD system. The solution of these equations is given by

$$\begin{aligned}\begin{pmatrix}\tilde{a}_p^m \\ \tilde{a}_x^d\end{pmatrix} &= \begin{pmatrix}1 & -C_{px}^{md} \\ -C_{xp}^{dm} & 1\end{pmatrix}^{-1}\begin{pmatrix}a_p^m \\ a_x^d\end{pmatrix} \\ &= \frac{1}{\Delta}\begin{pmatrix}1 & C_{px}^{md} \\ C_{xp}^{dm} & 1\end{pmatrix}\begin{pmatrix}a_p^m \\ a_x^d\end{pmatrix},\end{aligned} \tag{7}$$

where Δ is the determinant of the *coupling matrix* describing the MNP-NQD interaction, given explicitly by $\Delta = 1 - C_{px}^{md}C_{xp}^{dm}$. Equation (7) implies that (i) if a MNP has a *dark* plasmon mode (i.e., $a_p^m = 0$) by virtue of its interaction with the NQD, this dark mode can be indirectly excited[31] and (ii) as a result of the interaction, the NQD-MNP system may show new resonances that occur at frequencies for which Δ is a minimum.

In principle, the set of equations given in Eq. (7) describe all the phenomena that arises from the electrostatic coupling. However, the intricate interdependence of the electric fields implicit in these equations needs special attention. For instance, the electric field E that appears in $\alpha(\omega, E)$ of Eq. (5) is given by $\vec{\mathbf{E}} = \tilde{a}_p^m\vec{\mathbf{E}}_p^m$ [see Eq. (6)], which by using the result expressed in Eq. (7) for $\tilde{a}_p^m$ gives the next equation:

$$\vec{\mathbf{E}} = \tilde{a}_p^m\vec{\mathbf{E}}_p^m = \frac{a_p^m + C_{px}^{md}\, a_x^d}{\Delta}\vec{\mathbf{E}}_p^m. \tag{8}$$

In general, the coupling constants C_{px}^{md} and C_{xp}^{dm} can be written as products of a factor containing spectral information $[f_p^m(\omega)\alpha(\omega, \vec{\mathbf{E}})]$ and a factor describing the details of the geometry of the interacting system $[G_{px}^{md}G_{xp}^{dm}$, which arise from the "geometrical" part of Coulomb's law], that is, $C_{px}^{md}C_{xp}^{dm} = f_p^m(\omega)\alpha(\omega, \vec{\mathbf{E}})G_{px}^{md}G_{xp}^{dm}$ with which we rewrite our previous result as

$$\vec{\mathbf{E}} = \frac{a_p^m + C_{px}^{md}\, a_x^d}{1 - f_p^m(\omega)\alpha(\omega, \vec{\mathbf{E}})G_{px}^{md}G_{xp}^{dm}}\vec{\mathbf{E}}_p^m, \tag{9}$$

a nonlinear equation for the field $\vec{\mathbf{E}}$. Furthermore, as we will discuss later, $\alpha(\omega,\vec{\mathbf{E}})$ is not just trivially found by replacing $\vec{\mathbf{E}}_o$ with $\vec{\mathbf{E}}$ in Eq. (4).

A. Approximations

1. "Classical" coupling

When the magnitude of the incident electric field $|\vec{\mathbf{E}}_o|$ is low enough such that $\Omega_o \ll \omega$, according to Eq. (4), the polarizability of the NQD becomes independent of the electric field:

$$\alpha(\omega) \approx -\frac{\mu^2}{\epsilon_b \hbar}\frac{1}{(\omega-\tilde{\omega}_o^*)}, \tag{10}$$

a condition that introduces a number of simplifications as we now discuss.

The NQD-MNP resonance condition occurs when $\Delta = 0$ in Eq. (7), which leads to

$$1 = C_{pX}^{md} C_{Xp}^{dm} = f_p^m(\omega)\alpha(\omega) G_{pX}^{md} G_{Xp}^{dm}. \tag{11}$$

Close to the resonance frequency of the LSPR, $f_p^m(\omega)$ can be approximated as[23]

$$f_p^m(\omega) \approx -\frac{A_p^m}{(4\pi\epsilon_b)^2(\omega-\tilde{\omega}_p^m)}, \tag{12}$$

where $A_p^m = 2\gamma_p^m \epsilon_b^2 (\omega_p^m)^3/[(\gamma_p^m-1)^2\omega_P^2]$, ω_P is the bulk plasma frequency of the metal (within a Drude's model), and ω_p^m depends on γ_p^m.

With this in mind and using Eqs. (10) and (12), the resonance condition $1 = C_{pX}^{md} C_{Xp}^{dm}$ can be cast in the following form:

$$(\omega-\tilde{\omega}_p^m)(\omega-\tilde{\omega}_o^*) = g^2, \tag{13}$$

where as a shorthand notation, we have introduced

$$g^2 \equiv \frac{\mu^2}{\epsilon_b\hbar}\frac{A_p^m}{(4\pi\epsilon_b)^2} G_{px}^{md} G_{xp}^{dm}, \tag{14}$$

as an exciton-plasmon coupling constant. This constant depends on several material parameters, including the dipole moment of the optical transition in the NQD (μ), the surface plasmon resonance frequency of the MNP (implicit in A_p^m) the background (low frequency) dielectric constant ϵ_b, and on the geometry of the MNP-NQD interacting system through the factors $G_{px}^{md} G_{xp}^{dm}$.

Equation (13) predicts that the NQD-MNP new resonance frequencies are

$$\omega_\pm = \frac{\tilde{\omega}_p+\tilde{\omega}_o}{2} \pm \sqrt{g^2+(\tilde{\omega}_p-\tilde{\omega}_o)^2/16}. \tag{15}$$

A resonance splitting is observed only when $g^2 > (\Gamma_p+\Gamma_o)^2/16$, or equivalently, when the exciton-plasmon coupling exceeds the losses of the coupled system. This splitting may for instance be observed experimentally in the scattering spectrum of NQD-MNP coupled systems. The scattering cross section of the coupled system is given by $C_s = k^4/(6\pi E_o)|\vec{\mathbf{p}}|^2$, with $\vec{\mathbf{p}} = \tilde{a}_x^d \vec{\mathbf{p}}_x + \tilde{a}_p^m \vec{\mathbf{p}}_p$, a vector addition that involves $1/\Delta$, in accordance with Eq. (7).

According to Eq. (14), there are two sets of parameters that must be optimized in designing a strongly coupled MNP-NQD system (in the classical sense here considered): the geometrical configuration of the system and their material (spectral) properties. Geometrically, the coupling constant g can be increased by positioning several noninteracting NQDs around a single MNP.

When two NQDs with excitation amplitudes a_1^d and a_2^d are placed in the vicinity of a MNP, the excitation amplitudes of Eq. (7) are given by[28]

$$\begin{pmatrix}\tilde{a}_1^d\\ \tilde{a}_p^m\\ \tilde{a}_2^d\end{pmatrix} = \begin{pmatrix}1 & -C_{1p}^{dm} & 0\\ -C_{p1}^{md} & 1 & -C_{p2}^{md}\\ 0 & -C_{2p}^{md} & 1\end{pmatrix}^{-1}\begin{pmatrix}a_1^d\\ a_p^m\\ a_2^d\end{pmatrix}, \tag{16}$$

where the determinant of the coupling matrix is given by $\Delta = 1-[C_{p1}^{md}C_{1p}^{dm} + C_{p2}^{md}C_{2p}^{dm}]$.

Assuming the two NQDs to be identical, leads to the following simplification:

$$\Delta = 1-\alpha(\omega) f_p^m(\omega)\left[G_{p1}^{md}G_{1p}^{dm} + G_{p2}^{md}G_{2p}^{dm}\right]. \tag{17}$$

For this system of three particles, the resonance condition $\Delta = 0$ can be written with Eqs. (4) and (12) as

$$(\omega-\tilde{\omega}_p^m)(\omega-\tilde{\omega}_o^*) = \tilde{g}^2, \tag{18}$$

with $\tilde{g}^2 = \frac{\mu^2}{\hbar}\frac{A_p^m}{(4\pi\epsilon_b)^2}[G_{p1}^{md}G_{1p}^{dm} + G_{p2}^{md}G_{2p}^{dm}]$, which is the same coupling constant derived previously with the addition of the terms that need to be accounted for in describing the geometry of the interacting system.

As a result of the NQD-MNP interaction, the spectrum of the light emitted by the NQD and the decay rate of its excited state can be modified, effects that are not accounted for in the "classical" approximation presented in this section. In the next section, we present a semiclassical treatment of the coupling problem whereby we continue to treat the electric fields classically but we describe the NQD with the aid of quantum mechanics.

2. "Quantum" effects of coupling

Within the EEM, the induced dipole moment $\vec{\mathbf{p}}$ on a dielectric sphere is given by

$$\begin{aligned}\vec{\mathbf{p}} &= \sum_{i=1}^{3} a_x^k \cdot p_x^k = \sum_{i=1}^{3}\frac{\epsilon_b\alpha(\omega,E_o)}{\sqrt{V_s}}(\hat{x}_k\cdot\vec{\mathbf{E}}_o)\sqrt{V_s}\hat{x}_k\\ &= \epsilon_b\alpha(\omega,E_o)\vec{\mathbf{E}}_o,\end{aligned} \tag{19}$$

where we have used the definition of the excitation amplitude given by Eq. (3) and the dipole moments of a sphere:[28]

$$p_x^k = \sqrt{V_s}\hat{x}_k. \tag{20}$$

The magnitude of the dipole moment can also be evaluated as the following expectation value:

$$\langle\vec{\mathbf{p}}\rangle = \mathrm{Tr}\{\hat{p}\rho\}, \tag{21}$$

where ρ is the electronic density matrix of the sphere, which must satisfy the following equation of motion (Liouville

equation):

$$\dot{\rho} = -(i/\hbar)[\hat{H},\rho] - \Gamma\rho, \tag{22}$$

where $\hat{H}$ the Hamiltonian of the system and Γ is an operator that accounts for the rates of the processes that lead to electronic energy relaxation (in our study we only consider spontaneous emission). The Hamiltonian $\hat{H}$ is given by

$$\hat{H} = \hbar\omega_o - \hat{p}\cdot\vec{\mathbf{E}}'. \tag{23}$$

Here, $\hbar\omega_o$ is the energy of the transition between the ground ($|1\rangle$) and excited ($|2\rangle$) states of the emitter which for the sake of simplicity is assumed to be a two level system. Its dipole moment operator is assumed to consist of the nondiagonal elements: $\hat{p} = \mu(|2\rangle\langle 1| + |1\rangle\langle 2|)$, where μ is the transition dipole moment of the NQD. $\vec{\mathbf{E}}'$ is the total electric field that drives the emitter, which consists of the applied field $\vec{\mathbf{E}}_o$ plus the field produced by the MNP, given by Eq. (9). When the sphere is isolated from the MNPs, this field is simply given by $\vec{\mathbf{E}}_o$ and the resulting electronic polarizability is given by Eq. (4).

However, when the emitter interacts with MNPs, the electric field that produces electronic excitations [the nonlinear Eq. (9)] contains a contribution from $\alpha(\omega,E)$, the polarizability of the NQD to this electric field, which is the function that we aim to find by solving Eq. (22). In order to do so, we introduce in this section a number of approximations.

To begin, we expand the denominator of Eq. (9) as a Taylor series:

$$\frac{1}{1 - f_p^m(\omega)\alpha(\omega,E)G_{pX}^{md}G_{Xp}^{dm}} \approx 1 + f_p^m(\omega)\alpha(\omega,E)G_{pX}^{md}G_{Xp}^{dm} + \cdots, \tag{24}$$

yielding to zeroth order,

$$\vec{\mathbf{E}} \approx \left(a_p^m + C_{px}^{md}\,a_x^d\right)\vec{\mathbf{E}}_p^m. \tag{25}$$

The coupling factors G_{pX}^{md}, G_{Xp}^{dm} originate from the Coulomb interaction between the surface charge (surface dipole) eigenmodes of the interacting particles. Typically, when coupling takes place between particles of dissimilar dimensions, these geometrical coupling constants are small and when they are smaller than unity,[28] the Taylor expansion is justifiable.

Because of our initial long-wavelength assumption, $\vec{\mathbf{E}}_o$ is constant over the entire surface of the MNP which then allows us to simplify a_p^m :

$$\begin{aligned} a_p^m &= f_p^m(\omega)\oint \tau_p^m(\vec{\mathbf{r}})\hat{n}\cdot\vec{\mathbf{E}}_o\,dS, \\ &= f_p^m(\omega)\,\vec{\mathbf{p}}_p^m\cdot\vec{\mathbf{E}}_o, \end{aligned} \tag{26}$$

a scalar product of the dipole moment $\vec{\mathbf{p}}_p^m$ of the mth LSPR of the particle with the incident field.

With these results,

$$\begin{aligned} \vec{\mathbf{E}}' &= \vec{\mathbf{E}}_o + \left[f_p^m(\omega)\,\vec{\mathbf{p}}_p^m\cdot\vec{\mathbf{E}}_o + C_{px}^{md}\,a_x^d\right]\vec{\mathbf{E}}_p^m, \\ &= \vec{\mathbf{G}}_p^m|\vec{\mathbf{E}}_o| + \vec{\mathbf{F}}_p^m|\vec{\mathbf{p}}_x^d|, \end{aligned} \tag{27}$$

where we have defined the functions $\vec{\mathbf{G}}_p^m$ and $\vec{\mathbf{F}}_p^m$ as

$$\begin{aligned} \vec{\mathbf{G}}_p^m|\vec{\mathbf{E}}_o| &= \left[\hat{n}_e + f_p^m(\omega)\left(\vec{\mathbf{p}}_p^m\cdot\hat{n}_e\right)\vec{\mathbf{E}}_p^m\right]|\vec{\mathbf{E}}_o|, \\ \vec{\mathbf{F}}_p^m\,p_x^d &= \left(C_{px}^{md}\,\hat{a}_x^d\right)\vec{\mathbf{E}}_p^m|\vec{\mathbf{p}}_x^d|, \end{aligned} \tag{28}$$

with $\vec{\mathbf{p}}_x^d = |\vec{\mathbf{p}}_x^d|\hat{n}_x$, $\vec{\mathbf{E}}_o = |\vec{\mathbf{E}}_o|\hat{n}_e$, and $C_{px}^{md}\hat{a}_x^d$ the excitation amplitude of the LSPR mode m of particle p by a unit dipole $\hat{p}_x$. Both of these functions describe the effect of the MNP on the local electric field experienced by the NQD. $|\vec{\mathbf{p}}_x^d|$ is given by Eq. (21).

The dimensionless function $\vec{\mathbf{G}}_p^m$ contains information about how the MNP produces an electric field in response to the externally applied $\vec{\mathbf{E}}_o$, whereas the function $\vec{\mathbf{F}}_p^m$ describes the part of the electric field produced by the MNP due to excitation of LSPRs by the radiation emitted by the NQD's dipole. Clearly, when the NQD is isolated $\vec{\mathbf{G}}_p^m = 1$ and $\vec{\mathbf{F}}_p^m = 0$, and the polarizability $\alpha(\omega,E_o)$ of Eq. (4) is found after solving Eq. (22) (under steady-state conditions). Our interest is in finding ρ (and, consequently, α) by taking into account the self-interaction terms that arise from $\vec{\mathbf{F}}_p^m\,p_x^d$ in Eq. (27).

By using the rotating wave approximation,[29] the following coupled differential equations for the coherence ($\sigma_{12} = \rho_{12}e^{-i\omega t}$) and the excited state population (ρ_{22}) of the NQD are obtained from Eq. (22):

$$i\hbar\dot{\sigma}_{12} = \left[\hbar(\omega - \tilde{\omega}_o^*) - \mu^2 F_p^m n\right]\sigma_{12} - n\Omega_e \tag{29}$$

and

$$i\hbar\dot{\rho}_{22} = 2\mathrm{Im}(\Omega_e\sigma_{21}) - 2\mu^2\mathrm{Im}\left(F_p^m\right)\sigma_{12}\sigma_{21}, - i\hbar\Gamma\rho_{22} \tag{30}$$

with the population inversion n defined as $n = \rho_{22} - \rho_{11}$ and the normalisation condition $\rho_{11} + \rho_{22} = 1$ (closed system). The symbol ω is the frequency of the incident uniform electric field, $\hbar\Omega_e = \mu E_o G_p^m/2$ is the effective Rabi frequency, $\tilde{\omega}_o = \omega_o - i\Gamma/2$ is the complex electronic transition frequency of the emitter (with $\tilde{\omega}_o^*$ its complex conjugate) and $\sigma_{21} = (\sigma_{12})^*$.

These equations are similar to the optical Bloch equations of a two-level atom[29] except for the modulation of the Rabi frequency ($\Omega_o = \mu E_o/2\hbar$) by the function G_p^m and the terms $\mu^2 F_p^m n\sigma_{12}$ and $\mathrm{Im}(F_p^m)\sigma_{12}\sigma_{21}$. These terms involve the function F_p^m, that arises from the NQD self-interaction due to the induced electric fields on the plasmonic particles and the products $\sigma_{12}n$ and $\sigma_{12}\sigma_{21}$, which account for nonlinear and population-dependent effects. In atomic physics,[32,33] similar nonlinear terms appear in the Bloch equations for dense media and these have been shown to give rise to an array of phenomena including optical bistability, the nonlinear Fano effect, linear and nonlinear spectral shifts, and lasing without inversion.

3. Steady state

In steady state, the population of the excited state of the NQD is given by the following equation:

$$\begin{aligned} \rho_{22} &= \frac{|\hbar\Omega_e|^2}{|\hbar(\omega - \tilde{\omega}_c)|^2 + 2|\hbar\Omega_e|^2} \\ &= \frac{|\hbar\Omega_e|^2}{[\hbar(\omega - \omega_c)]^2 + (\hbar\Gamma_c/2)^2 + 2|\hbar\Omega_e|^2}, \end{aligned} \tag{31}$$

where for shorthand notation, we have defined a frequency $\tilde{\omega}_c = \omega_c - i\Gamma_c/2$ with $\omega_c = \omega_o + \mu^2\mathrm{Re}(F_p^m)n/\hbar$ and $\Gamma_c/2 = \Gamma/2 + \mu^2\mathrm{Im}(F_p^m)n/\hbar$. This frequency $\tilde{\omega}_c$ also depends on ρ_{22} ($n = \rho_{22} - \rho_{11}$) making Eq. (31) a transcendental one.

According to this equation, G_p^m expresses the modification (enhancement) of the Rabi frequency due to the electric fields

from the MNP. G_p^m modifies the Rabi frequency according to $\hbar\Omega_e = \mu E_0 G_p^m/2$. Effectively, the MNPs can "focus" electromagnetic energy to the NQD thus promoting more transitions between the ground and excited states. In affecting the excitation/relaxation dynamics of the dipole transition, the function F_p^m plays two roles: (i) according to Eq. (31), the real part is responsible for a spectral shift in the resonance of the NQD transition described by $\omega_c = \omega_o + \mu^2 \mathrm{Re}(F_p^m) n/\hbar$ and (ii) its imaginary part is responsible for changes in its decay lifetime, mathematically given by $\Gamma_c/2 = \Gamma/2 + \mu^2 \mathrm{Im}(F_p^m) n/\hbar$. The interplay of these two functions, namely G_p^m and F_p^m will determine the response of the excitation in the coupled system, which could result in irreversible energy transfer to the plasmon resonance of the MNPs (fluorescence quenching), fluorescence enhancement, etc.

In these two theory sections, we have considered the NQD-LSPR coupling at two approximation levels. In the following section, we consider the application of the results obtained to a few specific MNP-NQD systems, namely, the coupling of a single NQD to (i) a single Ag nanorod, (ii) a collection of coupled nanorods exhibiting plasmon hybridization, and (iii) the experiment of Anger *et al.*[34] consisting of the controlled coupling of a single molecule to an Au nanoparticle.

III. CASE STUDIES

A. Coupling to a single nanorod

1. "Classical" description

In Fig. 1, we show the scattering and absorption cross sections calculated for systems of coupled NQD-metal nanorod. The nanorod was assumed to be a hemispherically capped Ag cylinder of diameter 15 nm and length 80 nm, with a dielectric data for Ag that was adapted from Johnson and Christy.[35] Only the longitudinal (dipolar) LSPR was considered, for which $\gamma_p^m = 1.105$ equivalent to a wavelength of ~944 nm (1.314 eV). The dielectric spheres were assumed to have a diameter of 10 nm and a polarizabilty described by Eq. (10) with a resonance frequency that matched that of the LSPR of the nanorod and a width of 20 meV [that is $\tilde{\omega}_o^* = (1.314 + i0.01)$eV]. The edge to edge separation between the sphere and rod was 5 nm and the polarization of the incident (uniform) electric field was assumed to be parallel to the long axis of the nanorod.

For a value of $\mu^2/(V_s\epsilon_b) = 1/16$ ($\mu = 2.4\ e$nm $\approx 3.84 \times 10^{-28}$ Cm), the scattering spectra shown in Fig. 1 consists of a doublet with a "dip" located at the position of the maximum scattering intensity for the isolated nanorod. The interaction with the NQD is said to have induced a "transparency" in the scattering spectrum of the nanorod. When the single rod interacts with two NQDs positioned at both ends of its tips, the induced transparency is stronger as evidenced by an increased depth in the spectrum at the position of the LSPR of the noninteracting rod, a phenomenon that is consistent with our previous discussion leading to Eq. (18).

2. "Quantum" mechanical description

In Fig. 2, we show the spectra of $\vec{\mathbf{G}}_p^m$ and $\vec{\mathbf{F}}_p^m$ calculated (using the EEM) for a point located 20 nm away from a Ag nanorod. For this nanorod, the spectrum of the z component

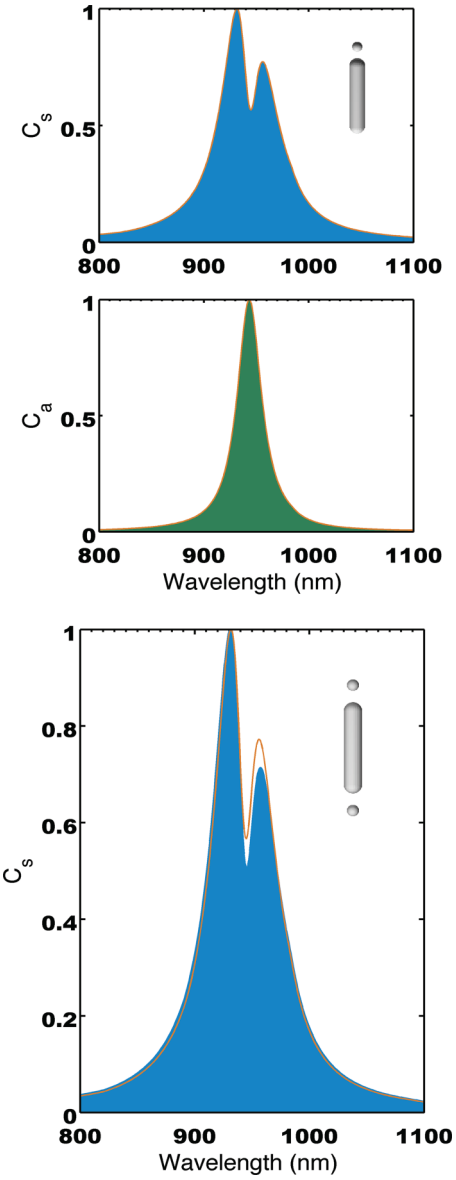

FIG. 1. (Color online) (Top) Spectra of the normalised scattering (C_s) and absorption (C_a) cross sections for a coupled system consisting of a single NQD with a single nanorod as indicated in the inset. (Bottom) Spectra of the normalised scattering (C_s) cross section for a system comprised of two noninteracting NQDs with a single nanorod (shaded plot) arranged as shown in the inset. Also shown for comparison is the spectrum of the case of a single NQD-nanorod case (line).

of $\vec{\mathbf{G}}_p^m$ is composed of two resonance features (at 943 and 477 nm), both corresponding to modes that can be excited by an incident uniform electric field. On the other hand, the spectrum of the z component of $\vec{\mathbf{F}}_p^m$ shows one additional resonance at 581 nm that corresponds to the first quadrupole-like mode of the nanorod. This mode is characterized by having $\vec{\mathbf{p}}_p^m = 0$ and therefore does not contribute to $\vec{\mathbf{G}}_p^m$ [see Eq. (28)].

These results have also been compared to finite element full-field simulations implemented in COMSOL MULTIPHYSICS and the spectral position of the maxima in the total radiated power. However, the position of the maximum in the spectrum

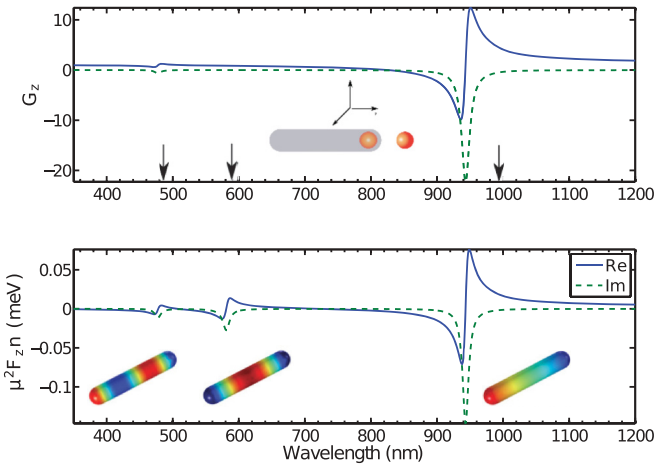

FIG. 2. (Color online) Plots of z components of (top) $\vec{\mathbf{G}}$ and (bottom) $\vec{\mathbf{F}}$ (assumed $\mu = 1$ $e$nm) calculated for a point located 20 nm away on the z plane from the tip of a 80 nm long, 15 nm in diameter Ag nanorod with $\epsilon_b = 2.25$ (z axis coincides with long axis of the nanorod). The dielectric data of Ref. 35 for Ag was used, and the first three LSP modes of the nanorod were taken into account [$\gamma_{\mathrm{NR}}^{m_1} = 1.105$ (477 nm), $\gamma_{\mathrm{NR}}^{m_2} = 1.358$ (582 nm), $\gamma_{\mathrm{NR}}^{m_3} = 1.713$ (943 nm)]. Also shown in the bottom are the surface charge distributions σ_{NR}^{m} of each of the modes considered. The arrows on the top panel indicate the position of the scattering spectrum calculated with COMSOL (485, 595, and 995 nm).

(longitudinal dipole mode) is located at 995 nm (shown with an arrow in Fig. 2) as opposed to the 943 nm predicted by the EEM. This discrepancy arises from the inclusion of retardation effects in the finite element calculations.

In Fig. 3, we show the calculated excited state population of a fictitious NQD positioned 20 nm away from one of the

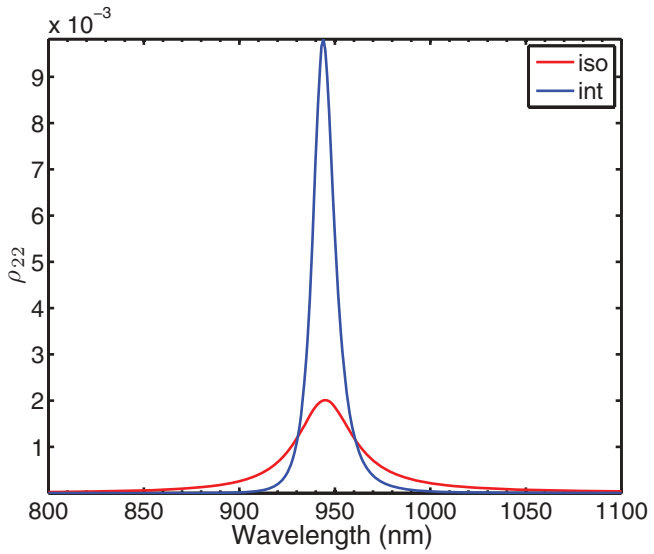

FIG. 3. (Color online) ρ_{22} calculated for a NQD positioned 20 nm away from the Ag nanorod as in Fig. 2. For this NQD, we have assumed $\hbar\omega_o = 1.312$ eV (945 nm) and $\hbar\Gamma = 50$ meV. "iso" is the excited state density for the isolated NQD, which for clarity, has been multiplied by 100. "int" corresponds to that of the interacting NQD. The incident field intensity was 10 kW/cm^2.

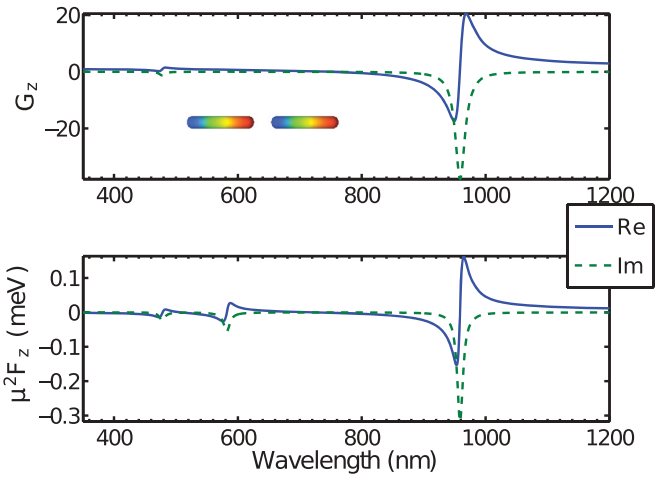

FIG. 4. (Color online) Spectra of G_z (top) and F_z (bottom) calculated at the center of a Ag nanorod dimer. The tip to tip separation is 20 nm, the z axis coincides with the long axis of the nanorods and the dimensions of each nanorod are those employed in Fig. 2. Also shown in this figure is the surface charge distribution of the lowest-order collective surface plasmon mode of the pair.

end tips of a Ag nanorod (same dimensions and orientation as in Fig. 2). For this calculation we have assumed the NQD's exciton transition to be resonant with the longitudinal dipole-like mode of the nanorod and furthermore, we have also assumed the NQD's excited state dipole to be parallel to the long axis of the nanorod. Under these conditions and according to Fig. 2 and Eq. (31) the main effect of the surface plasmon modes of the nanorod on the NQD is to enhance the excitation rate via an enhancement of the local electric field $\vec{\mathbf{E}}$ [see Eq. (27)] accounted for by the magnitude of $\vec{\mathbf{G}}_p^m$. As shown in this figure, the interaction leads to an enhancement of the excited state population.

B. Coupling to a dimer

According to Eqs. (27), (28), and (31), further enhancements in ρ_{22} can be achieved by increasing the magnitude of the dipole moments of the surface plasmon resonances. One way of achieving this is by exploiting collective surface plasmon modes of coupled MNPs. In Fig. 4, we show the spectra of G_z and F_z calculated in the center point of a nanorod dimer, separated by 20 nm (distance tip to tip) and in Fig. 5 the resulting spectra of ρ_{22} along with that of the isolated NQD.

Within the EEM, nanoparticle coupling leads to the formation of new collective LSPRs for which the dipole moments are linear combinations of those of the noninteracting particles. Similar to Eq. (1), the dipole moments are given by $\vec{\mathbf{p}} = \sum \tilde{a}_p^m \vec{\mathbf{p}}_p^m$, which for the case of the dimer of Fig. 4 (considering only the longitudinal dipole moment p_p^d of each nanorod) results in two combinations ($\vec{\mathbf{p}} \propto \vec{\mathbf{p}}_p^d \pm \vec{\mathbf{p}}_p^d$) one of which consists of an in-phase oscillation resulting in an increased dipole moment (collective bright mode). This bright mode leads to an increase in $|\vec{\mathbf{G}}|$ [see inset of Fig. 5 and Eq. (28)] and, therefore, in Ω_e, which bearing Eq. (31) in mind, translates in the enhanced excited state population shown in Fig. 5. Another consequence of coupling is a spectral shift

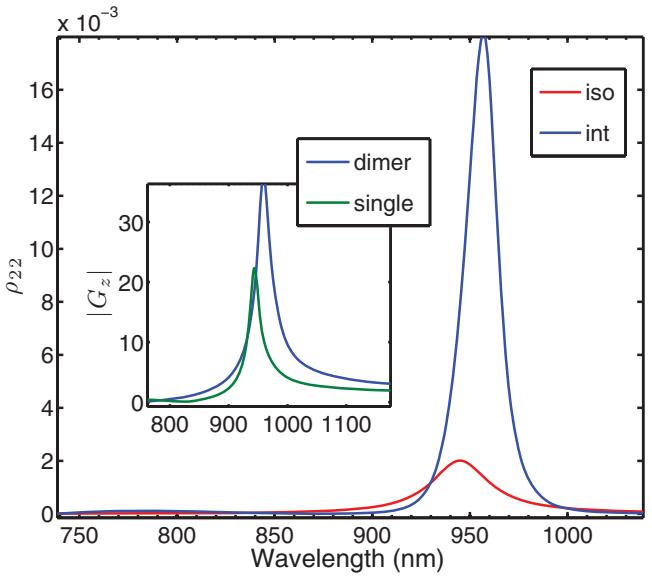

FIG. 5. (Color online) Spectrum of ρ_{22} calculated for a NQD positioned in the middle of the coupled Ag nanorod dimer of Fig. 4. For this NQD, we have assumed $\hbar\omega_o = 1.312$ eV (945 nm) and $\hbar\Gamma = 50$ meV. "iso" is the excited state density for the isolated NQD, which for clarity, has been multiplied by 100. The incident field intensity was 10 kW/cm^2. The inset shows the spectra of $|G_z|$ for the single nanorod and its dimer.

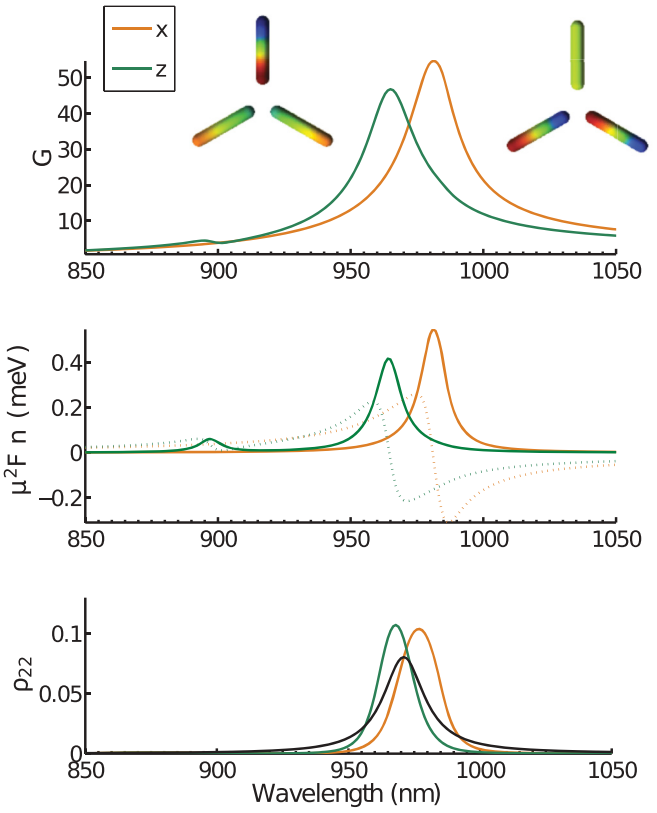

FIG. 6. (Color online) Response of a NQD [$\hbar\omega_o = 1.277$ eV (971 nm), $\hbar\Gamma_o = 25$ meV, $\mu = 1$ $e$nm] positioned in the center of a trimer of nanorods (same dimensions as in Fig. 2). The nanorods form an isosceles triangle and have two collective brigth LPS modes shown in the top. (Top) Plot of the magnitude of $\vec{\mathbf{G}}$ for illumination with x and z polarized light. (Middle) Plot of the real and imaginary (dotted line) parts of $\mu^2\vec{\mathbf{F}}n/\hbar$. (Bottom) Plots of the resulting spectra of the excited state population along with the one for the isolated NQD (black line, multiplied by 1000 for clarity).

in the resonance frequency of the collective modes [as evident in the inset of Fig. 5], an effect leading to a noticeable shift in the maximum of the spectrum of ρ_{22} that results from preferential excitation enhancements (described by the spectrum of $|\vec{\mathbf{G}}|$) over a particular spectral window.

The symmetry of the interacting MNPs plays an important role in determining the optical properties of the collective LSPRs,[27,36] leading to selection rules for their excitation by a uniform electric field. In Fig. 6, we consider the interaction of a fictitious NQD located in the center of a nanorod trimer forming an isosceles triangle (point group D_{3h}). For this geometrical arrangement, the two lowest-order bright LSPRs are oriented along two perpendicular directions: horizontal (x) and vertical (z), and can be excited by light with electric fields polarized on each direction.[27] Due to the asymmetry of the triangle on these two axes (the condition for an isosceles triangle), the two LSP modes have different resonance frequencies, a condition that is evident in the spectra of $\vec{\mathbf{G}}$. If the NQD's exciton transition spectrum encompasses these two LSP modes as is shown in Fig. 6 (bottom), then as the incident polarization is changed from x to z polarized, the MNP-NQD interaction would lead to a ρ_{22} that exhibits a peak amplitude on the red and blue end of the isolated NQD spectrum. This optical effect can be achieved with NQDs due to the isotropy of their excitation dipole moment.[37]

C. Effect of $\vec{\mathbf{F}}$

In the structures considered so far, the magnitude of $\mu^2\vec{\mathbf{F}}n/\hbar$ has been considerably smaller than the linewidth of the exciton transition, resulting in almost negligible effects from this interaction pathway. The effect of $\vec{\mathbf{F}}$ on the excited state population is nonlinear and intensity dependent. According to Eq. (31), it modifies ρ_{22} in two ways: it can lead to spectral shifts and it can modify the decay rate of the NQD, both effects are described by the real and imaginary parts of $\mu^2\vec{\mathbf{F}}n/\hbar$, which depend on $n = 2\rho_{22} - 1$ and therefore on the intensity of the applied field. For a plasmonic structure supporting dark modes, according to Eq. (28) $\vec{\mathbf{G}} = 1$ and $\vec{\mathbf{F}}$ has a spectrum whose line shape is given by Eq. (12) but with a magnitude dictated by the geometry of the MNP and the MNP-NQD coupled system.

In Fig. 7, we show the effect of an artificial spectrum of $\mu^2\vec{\mathbf{F}}/\hbar$ that was modeled to have a Lorentzian lineshape centered on the exciton transition energy of the NQD but whose magnitude was varied between 2Γ and $\Gamma/4$. In this situation, $\rho_{22}(\omega = \omega_o) = |\hbar\Omega_e|^2/[(\hbar\Gamma_c/2)^2 + 2|\hbar\Omega_e|^2]$, which attains a maximum value of 1/2 when $\Gamma_c = 0$ or when the coupling of the NQD to the LSPR leads to a loss compensation ($|\Gamma/2 + \mu^2\mathrm{Im}(F)n/\hbar|^2 = 0$).

As can be seen in Fig. 7, if the magnitude of $\mu^2\vec{\mathbf{F}}n/\hbar$ is larger than Γ, the MNP-NQD interaction leads to quenching of the excited state population. Physically, this results from an increased value of Γ_c which is interpreted as an increase in

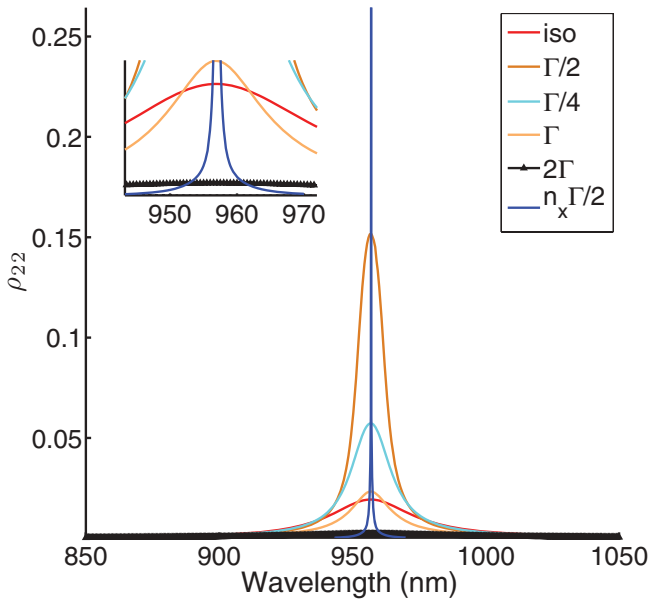

FIG. 7. (Color online) Effect of the peak amplitude (indicated in the legend) of $\mu^2\vec{\mathbf{F}}n/\hbar$ on the spectrum of ρ_{22}. "iso" refers to the isolated NQD. For this calculation we have assumed $\mu = 10$ $e$nm, $I = 1$ kW/cm^2 and $\hbar\Gamma = 5$ meV, $n_x = 1.74$.

energy dissipation in the NQD due to energy transfer to surface plasmon modes in the MNP. At the other extreme, maximum enhancement is observed at a peak amplitude of $\mu^2\vec{\mathbf{F}}n/\hbar$ that is slightly larger than $\Gamma/2$ (the line labeled $n_x\Gamma/2$ on the figure). The enhancement is accompanied with a significant decrease

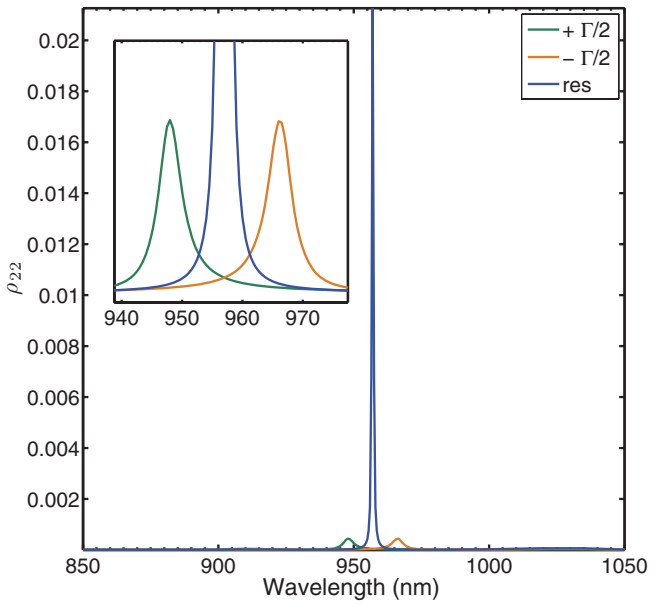

FIG. 8. (Color online) Effect of the resonance wavelength of the function $\vec{\mathbf{F}}$ on the spectra of ρ_{22}. Three cases are plotted and they consist of (i) a blue shift of $\Gamma/2$ in $\vec{\mathbf{F}}$, (ii) a redshift by the same amount, and (iii) the case of resonance considered already in Fig. 7. All the numerical parameters remained unchanged from those employed previously.

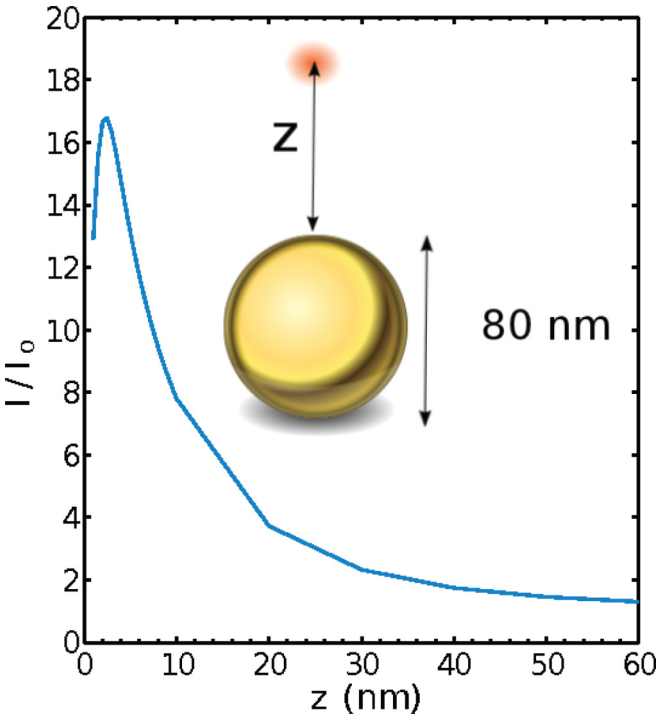

FIG. 9. (Color online) Relative emission intensity vs distance for a single emitter coupled to a Au nanosphere of 80 nm in diameter. For this calculation, we have employed the following set of parameters: $\hbar\omega_o = 2.39$ eV (518 nm) $\hbar\Gamma_o = 50$ meV, $\epsilon_b = 2.25$. $\mu = 48.5$ D. For these calculations, we have considered the first three LSP modes ($\gamma_p^l = 3, 5, 7$) of a sphere, each mode is $2l + 1$ degenerate.

in the spectral linewidth but the maximum value of ρ_{22} attained is still well below the 1/2 limit. This effect is independent of the linewidth of the function $\vec{\mathbf{F}}$ but depends strongly on the position of its resonance as demonstrated by the results of Fig. 8.

D. Comparison with experimental results

Anger *et al.*[34] have measured the emission intensity of single molecules as a function of separation distance z from a 80 nm in diameter Au sphere. In this study, a continuous increase in the measured fluorescence count rate was observed as z decreased up to an optimum value (maximum enhancement when $z = 5$ nm) after which it started to decrease sharply. In order to simulate the experimental conditions of Ref. 34, we considered a spherical Au nanoparticle of 80 nm in diameter and calculated, using Eq. (31), the excited state population and emission intensity I as a function of separation distance (I was calculated as $\int \rho_{22}(\omega)\, d\omega$ and is shown in the plot normalized to that of the isolated emitter). The results are shown in Fig. 9. Our results closely follow the experimental trends [see Fig. 4(a) of Ref. 34] albeit with an optimum distance that is about 50% smaller. Failure to reproduce the experimental data may arise from our complete neglect of substrate effects, which are known to modify the LSP resonances of nanoparticles,[38] retardation, and radiative damping, which are implicitly ignored in the EEM and furthermore, the inclusion of only the first three eigenmodes of the Au nanoparticle in describing the interaction. Additionally, we have assumed a value for μ

that may not coincide with the appropriate experimental value. At shorter molecule-MNP distances a full quantum mechanical treatment of the coupling is required in order to better describe the experimental results.[39]

IV. CONCLUSIONS

In summary, we have derived a semianalytical model to describe the coupling of an electronic excitation in a dipole emitter to the localized surface plasmon resonances of collection of metal nanoparticles. This interaction can lead to resonance splittings in the scattering spectrum of metallic nanostructures and also to enhancement or quenching of the excited state population of the emitter, effects that arise from a balance between the relative contributions from a pair of functions $\vec{\mathbf{G}}$ and $\vec{\mathbf{F}}$. Model calculations were presented to illustrate the applicability of our formalism, including an experimentally relevant case where we were able to reproduce the qualitative features of the interaction of a single molecule and a single Au nanoparticle. Due to its simple interpretation, the theory presented here can be used to design plasmonic-excitonic coupled structures, which are the building blocks of novel electro-optic technologies at the nanoscale.

ACKNOWLEDGMENTS

This work has been supported by the Australian Research Council under DP110101767, DP110101454, and DP110100221. D.E.G. would also like to acknowledge the Melbourne Materials Institute.

APPENDIX: THE EEM, THE ELECTRIC FIELD RADIATED BY THE NQD, AND THE EXCITATION OF LSPRs

The surface plasmon eigenmodes of the MNPs were calculated by numerically solving the eigenproblem:

$$\sigma_p^m(\vec{\mathbf{r}}) = \frac{\gamma_p^m}{2\pi} \oint \sigma_p^m(\vec{\mathbf{r}}_q) \frac{(\vec{\mathbf{r}} - \vec{\mathbf{r}}_q)}{|r - r_q|^3} \cdot \hat{n}\, dS_q, \tag{A1}$$

where γ_p^m are the eigenvalues that are related to the resonance wavelength of the surface plasmon modes by

$$\epsilon_M(\lambda_p^m) = \epsilon_b \frac{1 + \gamma_p^m}{1 - \gamma_p^m}, \tag{A2}$$

with λ_p^m given by the real part of this equation. Here, λ_p^m is the wavelength of the surface plasmon resonance, $\epsilon_M(\lambda)$ is the (wavelength-dependent) permittivity of the metal and ϵ_b that of the (uniform) background medium. For a single spherical nanoparticle, $\gamma_p^{m=1} = 3$ (dipolar mode, triply degenerate. $\gamma_p^{m=2} = 5$ corresponds to a qudrupolar mode with fivefold degeneracy) and this equation reduces to the familiar resonance condition $\epsilon_M(\lambda) = -2\epsilon_b$ (The Frölich mode). A similar eigenvalue equation also exists for the surface dipole distributions $\tau_p^m(\vec{\mathbf{r}})$.[23,26] Once the set of $\sigma_p^m(\vec{\mathbf{r}})$ and $\tau_p^m(\vec{\mathbf{r}})$ are known, the excitation amplitudes a_p^m are calculated for a given polarization of the applied electric field $\vec{\mathbf{E}}_o$.

In the near-field approximation (i.e., when the wavelength of the driving field is larger than any other relevant size scale), the electric field radiated by the NQD's dipole moment $\vec{\mathbf{p}}_x$ is given by

$$\vec{\mathbf{E}}_x^d(\vec{\mathbf{r}}) = \frac{3(\vec{\mathbf{p}}_x \cdot \hat{n})\hat{n} - \vec{\mathbf{p}}_x}{4\pi\epsilon_b\, |\vec{\mathbf{R}} - \vec{\mathbf{r}}|^3}, \tag{A3}$$

with $\hat{n}$ a normal vector pointing on the direction of the separation distance between the location of the NQD ($\vec{\mathbf{R}}$) and the point of observation ($\vec{\mathbf{r}}$). This expression can be inserted into Eq. (2) resulting in

$$f_p^m(\omega) \oint \tau_p^m(\vec{\mathbf{r}}_i) \left[\frac{3(\vec{\mathbf{p}}_x \cdot \hat{n})\hat{n}_i \cdot \hat{n} - \hat{n}_i \cdot \vec{\mathbf{p}}_x}{4\pi\epsilon_b\, |\vec{\mathbf{R}} - \vec{\mathbf{r}}|^3} \right] dS = C_{px}^{md} \tilde{a}_x^d, \tag{A4}$$

where we have written $\vec{\mathbf{p}}_x = \tilde{a}_x^s \vec{\mathbf{p}}_x^d$ in accordance with Sec. II A2.

From this last result, one can infer by inspection that the coupling coefficient can be factored out as a product of a frequency-dependent component and a geometrical component:

$$\begin{aligned} C_{px}^{md} &= \frac{f_p^m(\omega)}{4\pi\epsilon_b} G_{px}^{md} \\ &= \frac{f_p^m(\omega)}{4\pi\epsilon_b} \oint \tau_p^m(\vec{\mathbf{r}}_i) \left[\frac{3(\vec{\mathbf{p}}_x^d \cdot \hat{n})\hat{n}_i \cdot \hat{n} - \hat{n}_i \cdot \vec{\mathbf{p}}_x^d}{|\vec{\mathbf{R}} - \vec{\mathbf{r}}|^3} \right] dS. \end{aligned} \tag{A5}$$

*dgomez@unimelb.edu.au; daniel.gomez@csiro.au

[1] S. Maier, *Plasmonics: Fundamentals and Applications* (Springer, New York, 2007).
[2] W. L. Barnes, A. Dereux, and T. W. Ebbesen, Nature (London) **424**, 824 (2003).
[3] M. Moskovits, L.-L. Tay, J. Yang, and T. Haslett, Top. Appl. Phys. **82**, 215 (2002).
[4] A. M. Michaels, J. Jiang, and L. Brus, J. Phys. Chem. B **104**, 11965 (2000).
[5] T. W. Ebbesen, H. J. Lezec, H. F. Ghaemi, T. Thio, and P. A. Wolff, Nature (London) **391**, 667 (1998).
[6] V. Shalaev, W. Cai, U. Chettiar, H. Yuan, A. Sarychev, V. Drachev, and A. Kildishev, Opt. Lett. **30**, 3356 (2005).
[7] V. Shalaev, Nat. Photon. **1**, 41 (2007).
[8] N. Liu, L. Langguth, T. Weiss, J. Kastel, M. Fleischhauer, T. Pfau, and H. Giessen, Nat. Mater. **8**, 758 (2009).
[9] J. B. Pendry and S. A. Maier, Phys. Rev. Lett. **107**, 259703 (2011).
[10] S. Wuestner, A. Pusch, K. L. Tsakmakidis, J. M. Hamm, and O. Hess, Phys. Rev. Lett. **107**, 259701 (2011).
[11] S. Wuestner, A. Pusch, K. L. Tsakmakidis, J. M. Hamm, and O. Hess, Phys. Rev. Lett. **105**, 127401 (2010).
[12] I. De Leon and P. Berini, Nat. Photon. **4**, 382 (2010).
[13] M. I. Stockman, Phys. Rev. Lett. **106**, 156802 (2011).
[14] R. R. Chance, A. Prock, and R. Silbey, in *Advances in Chemical Physics*, edited by S. A. R. I. Prigogine, Vol. 37 (Wiley InterScience, 1978), pp. 1–65.

[15]W. Zhang, A. O. Govorov, and G. W. Bryant, Phys. Rev. Lett. **97**, 146804 (2006).
[16]A. Govorov, G. Bryant, W. Zhang, T. Skeini, J. Lee, N. Kotov, J. Slocik, and R. Naik, Nano Lett. **6**, 984 (2006).
[17]A. O. Govorov, J. Lee, and N. A. Kotov, Phys. Rev. B **76**, 125308 (2007).
[18]J.-Y. Yan, W. Zhang, S. Duan, X.-G. Zhao, and A. O. Govorov, Phys. Rev. B **77**, 165301 (2008).
[19]R. D. Artuso and G. W. Bryant, Nano Lett. (2008).
[20]S. M. Sadeghi, Phys. Rev. B **79**, 233309 (2009).
[21]T. Ambjornsson, G. Mukhopadhyay, S. P. Apell, and M. Kall, Phys. Rev. B **73**, 085412 (2006).
[22]R. D. Artuso, G. W. Bryant, A. Garcia-Etxarri, and J. Aizpurua, Phys. Rev. B **83**, 235406 (2011).
[23]T. J. Davis, D. E. Gómez, and K. C. Vernon, Nano Lett. **10**, 2618 (2010).
[24]E. Prodan, C. Radloff, N. J. Halas, and P. Nordlander, Science **302**, 419 (2003).
[25]I. D. Mayergoyz, D. R. Fredkin, and Z. Zhang, Phys. Rev. B **72**, 155412 (2005).
[26]T. J. Davis, K. C. Vernon, and D. E. Gómez, Phys. Rev. B **79**, 155423 (2009), also in: Vir. J. Nan. Sci. & Tech. **19**, 17 (2009).
[27]D. E. Gómez, K. C. Vernon, and T. J. Davis, Phys. Rev. B **81**, 075414 (2010).
[28]T. J. Davis, D. E. Gómez, and K. C. Vernon, Phys. Rev. B **81**, 045432 (2010), also in: Vir. J. Nan. Sci. & Tech. **21**, 7 (2010).
[29]C. Cohen-Tannoudji, J. Dupont-Roc, and G. Grynberg, *Atom-Photon Interactions* (Wiley, 1998).
[30]D. Ricard, M. Ghanassi, and M. Schanne-Klein, Opt. Commun. **108**, 311 (1994).
[31]M. Liu, T.-W. Lee, S. K. Gray, P. Guyot-Sionnest, and M. Pelton, Phys. Rev. Lett. **102**, 107401 (2009).
[32]C. M. Bowden and J. P. Dowling, Phys. Rev. A **47**, 1247 (1993).
[33]M. E. Crenshaw and C. M. Bowden, Phys. Rev. A **53**, 1139 (1996).
[34]P. Anger, P. Bharadwaj, and L. Novotny, Phys. Rev. Lett. **96**, 113002 (2006).
[35]P. B. Johnson and R. W. Christy, Phys. Rev. B **6**, 4370 (1972).
[36]D. W. Brandl, N. A. Mirin, and P. Nordlander, J. Phys. Chem. B **110**, 12302 (2006).
[37]A. I. Chizhik, A. M. Chizhik, D. Khoptyar, S. Bär, and A. J. Meixner, Nano Lett. **11**, 1131 (2011).
[38]K. C. Vernon, A. M. Funston, C. Novo, D. E. Gómez, P. Mulvaney, and T. J. Davis, Nano Lett. **10**, 2080 (2010).
[39]A. Manjavacas, F. J. G. d. Abajo, and P. Nordlander, Nano Lett. **11**, 2318 (2011).